Gas-Filled Cavity Structures and Local Void Fraction Distribution in Aerated Stirred Vessel

A. Bombač, I. Žun, and B. Filipič
Lab. for Fluid Dynamics and Thermodynamics, Faculty of Mechanical Engineering

M. Žumer
Faculty of Chemistry and Chemical Technology
University of Ljubljana, Slovenia

The local structural function obtained by a microresistivity probe at different hydrodynamic regimes is examined. The structures, such as the vortex-clinging structure, the appearance of one and two large cavities, small 3-3 structure, large 3-3 structure, and ragged cavities were recognized by frequency transformation of the time-domain structural function. An optimized phase discrimination in signal processing was used. The distribution of the local void fraction (α) in a pilot-size stirred tank was experimentally investigated, because almost no such data can be found in the literature. The two-phase mixture was composed of air and water; α was measured at 190 nodes in the vertical half-section plane of the vessel. Relative differences smaller than 9% between integrated values of α and measured gas holdups agreed reasonably well under all conditions.

Introduction

The desire to identify flow fields in agitated chemical reactors in order to improve the processes of heat and mass transfer, or to affect biochemical processes, has attracted a number of researchers in the past two decades. A large body of knowledge has been developed to enable the predictions of flow regimes in relatively simple arrangements, such as vessels stirred by a single Rushton impeller. When operating in gas-liquid mixtures, Rushton impellers develop ventilated cavities behind the blades. Gas-filled cavity structures control energy dissipation, spatial gas-phase distribution in the liquid bulk, flooding conditions, and so on. In general, the form and configuration of gas-filled cavity structures is dependent on transport properties (Takahashi and Nienow, 1992), gas-flow rate and impeller speed, and the number of blades (Warmoeskerken and Smith, 1982). It appears from the literature, however, that even for a rather simple setup some indistinctness can be found regarding the transition from the VC structure to the structure of large cavities. For example, the structures with one and two large cavities were not identified in such cases (Ismail et al., 1984; Nienow et al., 1985; Warmoeskerken and Smith, 1985). On the other hand, the above structures were recognized by the transition from VC structure to structure with one, two, or up to six large cavities (Bruijn et al., 1974), or by the transition from VC structure to structures with one, two and three large cavities (Lu and Ju, 1989), followed by a very gradual transition to six large cavities (Warmoeskerken and Smith, 1982). Impeller gas-filled cavities were usually measured using a derotational technique combined with a video camera and flash photography (Bruijn et al., 1974; Warmoeskerken and Smith, 1982; Ismail et al., 1984), vibrating vane (Smith et al., 1987), hydrophones (de More, 1988), or CTA (Lu and Ju, 1989).

Most research of gas dispersion in stirred vessels has been oriented towards the study of global parameters such as power consumption, gas holdup, and mass-transfer rate. Unfortunately, almost no systematic data on local void fraction (α) distributions can be found in the literature. Experimental determinations of α can be provided by any physical principle for which the liquid and gas behaviors are distinct. One of the earliest methods of void fraction measurements by gas dispersion in a stirred tank was the vacuum sampling technique (Nienow et al., 1977). Nagase and Yasui (1983) modified this method by incorporating in a pair of resistivity probes for α and local bubble size measurements, and Barigou and Greaves (1992) by incorporating in two pairs of LED/photo

B. Filipič is also with the Dept. of Intelligent Systems, Jožef Stefan Institute, Ljubljana, Slovenia.

transistor detectors. Impedance probes take advantage of the change of either resistivity or capacitance according to the phase considered. These probes are widely used due to probe and circuitry simplicity which enable homemade products at low costs. de Figueiredo and Calderbank (1979) used such probes to determine the bubble-size distribution in an aerated stirred tank. Probe tips are normally of small diameters, and enable detection of very small bubbles. The first optical probes based on the different refractive index of phases (cited by Cartellier and Achard, 1991) were developed at the end of the 1960s. Frijlink (1987) used this type of probe for local void fraction measurements in gassed suspension reactors, while Bakker and van den Akker (1991) used it for verification of their computational fluid dynamic (CFD) simulation of α in a gassed stirred tank. Recently, the two-phase hydrodynamic characteristics were presented using CFD by Gosmann et al. (1992), Ranade and van den Akker (1994), and Morud and Hjertager (1996).

In the case of air dispersion in an aerated stirred vessel, a resistivity probe (R-probe) producing structural function M_p as described in Žun et al. (1995) was found to be simple and quite appropriate for detecting the local phase at low costs. The objective of this article is therefore to present the cavity structures recognized by the transformation of the M_p given by the R-probe into the frequency domain, as well as to determine the distribution of α in the liquid bulk of an aerated stirred tank. The experimental method was based on the local detection of gas filled cavities (Bombač, 1994). The void fraction scalar measurements by the R-probe, which are insensitive to the flow direction (unlike the CTA) or invariant to the transparency of the two-phase mixture (if compared to LDA), proved the method to be simple and effective.

The following cavity structures were recognized: vortex-clinging structure *VC*, the appearance of the first large cavity *1L*, two large cavities *2L*, small '3-3' structure *S33*, large '3-3' structure *L33* and ragged cavities *RC*. The transition from *VC* to *S33* structure runs successively over structures *1L* and *2L*, which results in a wider corresponding area in the map than evident from the literature. A cavity structure may include one, two, three or six large cavities which correspond to the *1L*, *2L*, *S33* and *L33* structures, respectively. Structures with four or five large cavities were not detected in any hydrodynamic regime. In the *2L* structure, a large cavity was followed by two vortex or clinging cavities. In the *S33* and *L33* structures, two or three large cavities were never detected on adjacent blades; they were always separated by smaller cavities. Large cavities were present on the same blades over longer observation periods.

A phase discrimination procedure based on optimization of threshold settings via genetic algorithms was applied in void fraction measurements at 190 nodes in the vertical half-section plane of the vessel. Spatial distributions of α are presented for the following hydrodynamic regimes: vortex-clinging, small '3-3' and large '3-3' structures, and two types of spargers, annular and ring sparger. The insensitivity of the R-probe to two-phase flow direction over a wide impact angle $\theta \leq \pm 90°$ enabled reasonable accuracy of measured α and reproducibility. From the contours of α, an influence of gravitational force acting perpendicular to radial discharge force can be recognized in all regimes, as well as areas of remarkably high gas-phase concentration and dead zones. Two-phase circulation loops can be recognized from the peaking of radially integrated α. A comparison of measured constant α contour pattern with the pattern obtained by numerical simulations in similar conditions (Bakker and van den Akker, 1991) is presented and discussed.

Experimental Technique

The experiment was carried out in a cylindrical perspex vessel of diameter 450 mm, flat-bottomed with rounded edges, of radius 75 mm. Four baffles of width T/12 were mounted perpendicular to the vessel wall with a gap of 7 mm. The geometry of the stirred vessel is depicted in Figure 1. Compressed air and demineralized water at room temperature were used in all experiments. The clearance c of the Rushton impeller was set to one-third or one-fourth of vessel size in the case of annular sparger or ring sparger, respectively. The ring sparger was made of rolled brass tubing of inner diameter 12 mm and had 80 equidistantly drilled holes of diameter 2 mm on the top side.

The impeller was driven by a 5 kW three-phase induction motor controlled by a frequency regulator, as shown in Figure 2. Impeller speed was measured with an infrared reflection counter while the impeller torque was measured using an in-line, precisely calibrated HBM torque transducer of accuracy class 1. Volumetric air-flow rates were measured by calibrated rotameters of accuracy class 2 (TG 300, MLW), corrected for pressure losses. The measurements of gas holdup were based on the change of the liquid height in the vessel by the method described in work of Rushton and Bimbinet (1968). At least 21 measurements of gas holdup were obtained for each hydrodynamic regime with a relative reproducibility error of less than 5%.

Basically, in a two-phase flow field, there are three states p possible at a particular point x at any time t: the liquid phase L, gas phase G, or phase interface S (Ishii, 1975). The corresponding structural function M_p is defined as

$$M_p(x,t) = \begin{cases} 1, & x \text{ is occupied by } p \\ 0, & x \text{ is not occupied by } p, \end{cases} \quad p = \{L, G, S\} \quad (1)$$

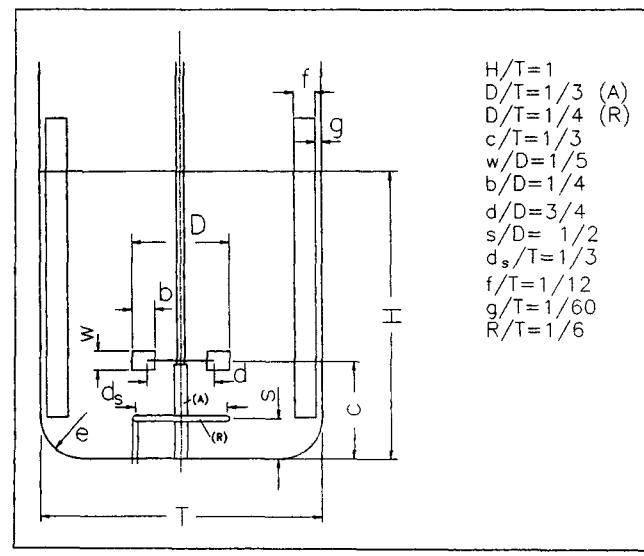

Figure 1. Geometrical parameters of stirred vessel.

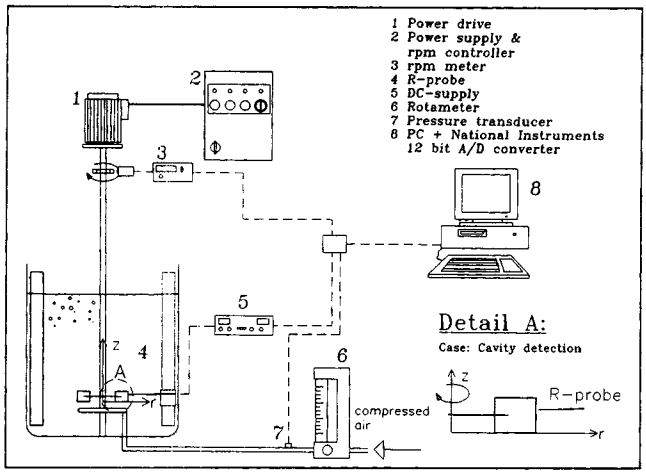

Figure 2. Experimental setup.

Detecting the phases by resistivity probe, the structural function M_p in this work is presented by changing voltage response.

Local detection of gas-filled cavity structures

The probe of 11-μm tip diameter was mounted on the baffle support very close to the outer impeller blades at $(r, z) = (75.5, 22)$ mm, where the appearance of the gas phase is most probable (Bombač and Žun, 1992). Each cavity transition over the probe tip was evident from the structural function as a pulse, the length of which was proportional to the cavity size (at constant impeller speed). As can be seen from Bruijn et al. (1974), a gas-filled cavity is a space filled with gas and attached to the back side of the blade. The cavity edge extends the impeller diameter, so any transition of the cavity over the measuring point corresponds to voltage pulse response. Depending on the cavity form, such as vortex-clinging or large cavity, the pulse length at const. impeller speed is proportional to the detected cavity size. The pulse length of a large cavity is a few times larger than the pulse length of a vortex or clinging cavity. It has been shown to be a very appropriate method for investigation of cavity presence in particular blade and cavity structure recognition.

Frequency analysis of the structural function M_p by discrete Fourier transformation enabled the presentation of the significant frequencies of an appearing gas phase (Žun et al., 1993). The Fourier coefficients X_k of a set consisting of N successive values $M_p(t_k)$, $k = 0, \ldots, N-1$, were obtained from

$$X_k = \Delta t \sum_{i=0}^{N-1} M_p(t_i) e^{-\frac{j2\pi ik}{N}} \tag{2}$$

where Δt denotes the time interval between successive instants t_i. Each Fourier coefficient X_k corresponds to the frequency $k/N\Delta t$. According to the Nyquist criterion, only coefficients from $k = 0$ to $k = N/2 - 1$ are meaningful. The power spectral density functions (PSDF) of the sequence M_p may then be calculated from the moduli of Fourier coefficients. Fourier transformation of structural functions was executed using the Fast-Fourier Transform algorithm.

The probe was powered by 5-V DC which produced a response magnitude of 2.3 V. Data acquisition was carried out using a 12-bit A/D *Lab-PC* card mounted on a PC-80486 supported by *LabWindows* software, both by National Instruments. The personal computer functioned as a central data acquisition device and data storage. The data acquisition rate was set to 5 kHz at 3 min of sampling duration per each run for local void fraction measurements, and 500 Hz at 1 min of sampling duration for gas-filled cavity detection. At the lowest impeller speed, at least 600 cavities were detected for further statistical treatment. Measurements were always performed in the same manner, starting from low to high impeller speeds, with stepwise increasing of the gas-flow rate at constant impeller speed.

α measurements

The structural function M_p was detected in the r-z vertical half-plane of a stirred vessel with the azimuth $\phi = 12°$ off the baffle. The area between the shaft and the vessel wall was divided into a mesh of 19×30 mm. The impeller region, in which bubble generation takes place and where most of the mass transfer has been shown to occur, was condensed in the z direction to 15 mm, to give a total of 190 measurement points nodes. M_p was detected in different hydrodynamic regimes and with two types of spargers, annular and ring. The former was used to eliminate, as much as possible, free undispersed gas and to enable measurements under the impeller. A ring sparger and impeller clearance of $H/4$ was chosen to enable comparison with results of other authors.

The local void fraction under stationary conditions is given by

$$\alpha(x) = \lim_{\Delta t \to \infty} \frac{1}{\Delta t} \lim_{\delta \to 0} \int_t^{t+\Delta t} M_G(x,t)dt \tag{3}$$

where Δt denotes total sampling time and δ interfacial thickness. A discrimination procedure transforms the R-probe response into a binary signal. Introducing the gas bubble residence time (s) Δt_{G_i}, Eq. 2 yields

$$\alpha(x) = \lim_{\Delta t \to \infty} \frac{\Sigma_i \Delta t_{G_i}}{\Delta t}. \tag{4}$$

See Figure 3.

Mapping of a raw signal M_p into a binary signal, which indicates the phases, also involves weak phase discrimination criteria. Particularly in dispersed flows, the deformation of phase interface at a sensor leads to a lag between the occurrence and the detection of the event due to hydrodynamic response time, and even more, the sensor may also deflect or alter the flow. To discriminate the phases, signal processing was used as developed in bubbly flow studies in simple conduits using a phase discrimination technique called man-machine discrimination Žun et al. (1995). The technique imitates human skill in reconstructing a binary signal, denoting the local appearance of the two phases from a raw probe signal. Development of the technique consists of three steps: the design of a general phase discrimination procedure, pro-

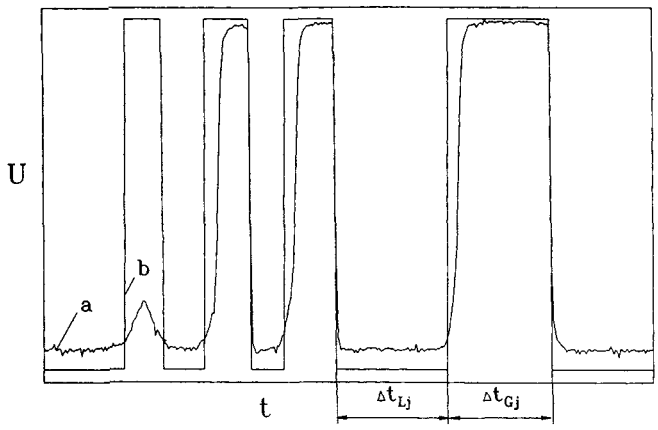

Figure 3. (a) R-probe response; (b) reconstructed binary signal.

viding raw and binary training signals, and tuning the discrimination procedure thresholds.

In adjusting the man-machine technique for discrimination of phases in a stirred tank, a training probe signal consisting of 40,000 samples and corresponding to 8 s of recording time was used. Through threshold optimization, the two-threshold version of the discrimination procedure turned out to be sufficient for adequate signal processing. The optimal threshold values found were 3.5% of the signal amplitude for the liquid-to-gas threshold and 25% for the gas-to-liquid threshold.

Results and Discussion

Gas-filled cavity recognition

Phase detection was carried out in the discharge flow as shown in Figure 2. At a chosen impeller speed $n_1 = \text{const.}$, the gas-flow rate was increased stepwise from q_1, q_2, q_3 to the point at which the impeller was no longer able to disperse air. At each setting of (n_i, q_j) after a fully developed regime was achieved, a structural function was recorded. After increasing the impeller speed to n_2 (s^{-1}), the procedure was repeated. In this manner ca. 260 measurements were taken and transformed into the frequency domain.

From the photography taken by Bruijn et al. (1974), Takahashi and Nienow (1992), and van't Riet and Smith (1973) in vortex and clinging cavity structures, it can be seen that the cavities are present on all blades and follow each other. Similar conclusions were found from the probe response. Transforming the time-domain structural function to the frequency-domain gives a significant blade frequency f_b, which is equal to the product of rotational impeller speed n and the number of blades z (see Figure 4). Among other Fourier coefficients, other significant subharmonics (f_b/z, $z = 1,2,\ldots,6$)

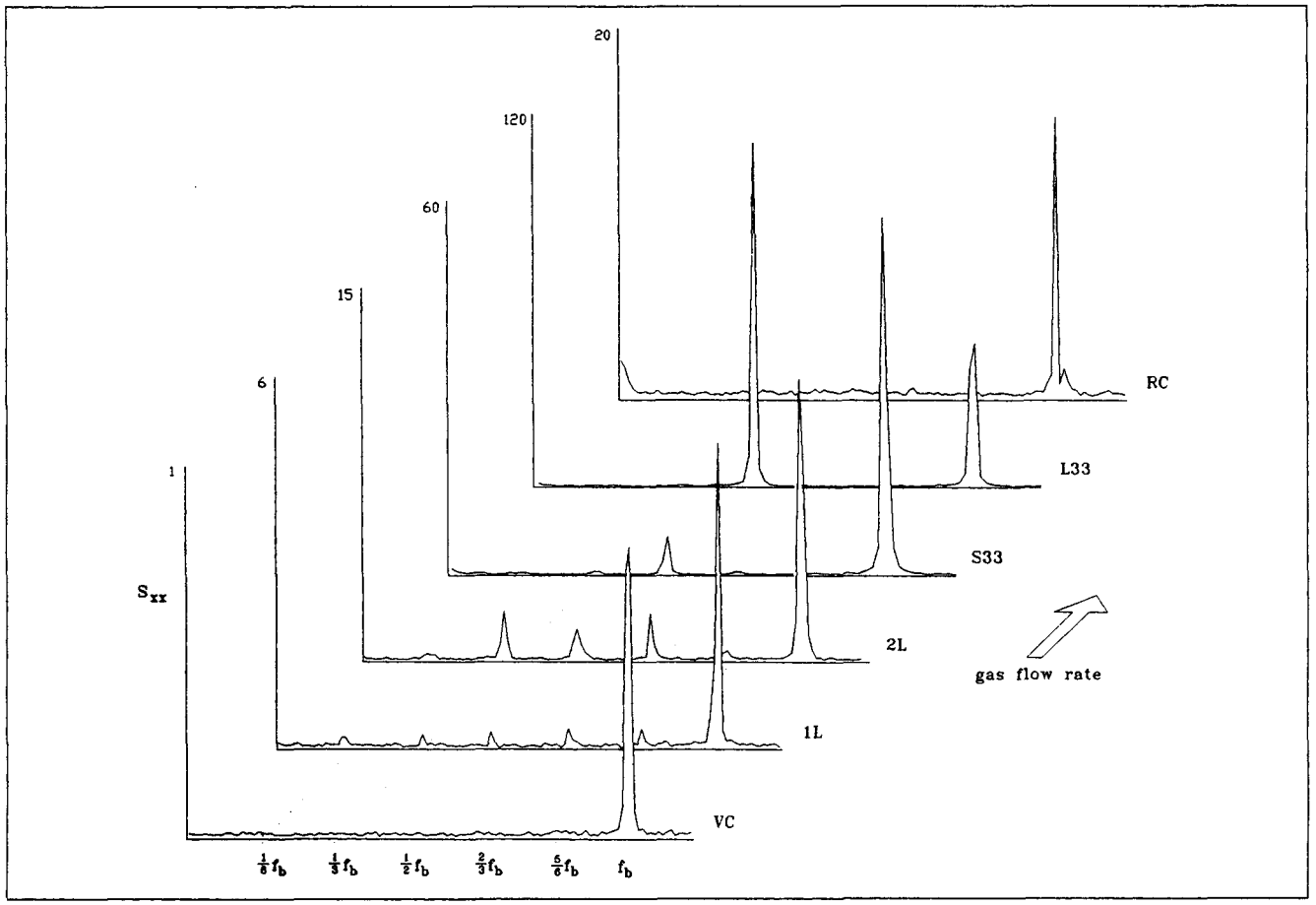

Figure 4. Frequency transformation of local structural function by different cavity structures.

could not be found. Such a pattern was recognized as a vortex-clinging structure (VC).

Increasing the gas-flow rate enlarges the clinging cavities up to the moment when the first large cavity is formed. The pulse length of the large cavity was in this case a few times longer than the rest of the pulses. Analysis of cavity presence on the same blade over longer periods proved that a large cavity appeared on various blades randomly; it moved from blade to blade. In the frequency domain the random appearing of large cavities on various blades corresponds to the rise of significant subharmonics $f_b/6$, $f_b/3$, $f_b/2$, $2f_b/3$ and $5f_b/6$, as shown in Figure 4. The pattern was recognized as the appearance of the first large cavity ($1L$).

Further increasing of gas-flow rates leads to formation of two large cavities. Cavities follow each other in the same sequence; one large cavity is followed by two vortex-clinging cavities, and so on. Such a configuration was present for a short time, only a few impeller revolutions, then two cavities appeared on the other blades, but never on adjacent blades. In the frequency domain two significant subharmonics predominate, $f_b/3$ and $2f_b/3$, respectively, as shown in Figure 4. The structure was recognized as the appearance of two large cavities ($2L$), and was not conditioned by a steady presence on the same blades. Lu and Ju (1989) investigated impeller discharge flow using a constant temperature anemometer (CTA). They found out that large cavities of $1L$ and $2L$ structures existed steadily on the same blade at lower impeller speeds, while at higher speeds they shifted their position to other blades.

A Rushton impeller with six blades normally operates with the '3-3' structure when used in industrial applications. In general, the term '3-3' structure includes the small '3-3' structure ($S33$) and large '3-3' structure ($L33$). Both are dependent on gas-flow rate. The $S33$ structure is described in literature (Bruijn et al., 1974; van't Riet and Smith, 1973) as a combination of three large and three clinging cavities. From the response over longer periods of observation, it was evident that large cavities were present on the same blades. The beginning of the $S33$ structure in the frequency-domain can be seen from the appearance of a significant Fourier coefficient at frequency $f_b/2$, which rises in accordance with increasing of the gas-flow rate. This pattern was taken as a criterion of $S33$ structure recognition. Similar findings were obtained by Smith et al. (1987) on the basis of the frequency analyses of pressure pulses on the vessel wall, especially the transition to the '3-3' alternating large-small cavities.

The $L33$ structure is, according to Nienow (1990) and Warmoeskerken and Smith (1982), a combination of three smaller and three larger large cavities, that is, a combination of large cavities exclusively. The alternating sequence of smaller and larger large cavities was also quite evident in the $L33$ structure. From the evolution of Fourier coefficients in the frequency domain (with increasing gas-flow rate), a rise of the coefficient at $f_b/2$ is obvious. At the point when both coefficients $f_b/2$ and f_b are nearly equal, the $L33$ structure was recognized, as depicted in Figure 4.

Since the vast majority of industrial-scale operations take place in the large cavity regime (Smith, 1991), the prediction of hydrodynamic regimes at which flooding may occur is of great importance. Flooding has often been explained in literature as a transition to unsatisfactory operation of an impeller in a gas-liquid system. According to Warmoeskerken and Smith (1985), the stable $L33$ structure reverts to six symmetrical clinging cavities, and at higher impeller speeds the changeover passes through a regime with six large cavities of identical size, which are described as violently vibrating, that is, ragged cavities (Nienow, 1990).

The last evident change in the structures, as can be seen from the evolution of the time-domain response as well as the frequency domain, was the transition from $L33$ to the ragged cavities structure (RC). The cavities were of different sizes with sporadic appearance of larger cavities. At higher gas-flow rates, a longer absence of any cavity on a particular blade was also possible when observing over longer periods of observation. A significant pattern of Fourier coefficients under the flooded condition is also depicted in Figure 4. From the Fouier coefficient as well as from the raw signal, it can be concluded that cavities of identical size appear randomly, or that the cavities present on all blades are of different size, or a combination of the two.

The reproducibility of the above mentioned method was checked for the hydrodynamic regimes corresponding to the VC, $1L$, $2L$, $S33$, $L33$, and RC structures. At impeller speed $n = 6.27\text{s}^{-1}$, by which all structures can appear, cavity detection measurement was repeated 7 times. All structures were repeatedly recognized in all cases.

Flow regime map

A coherent classification of the cavity structures developed by a single disk impeller can be given in a flow regime map such as the one given by Warmoeskerken and Smith (1986). This map was given in the dimensionless *Froude-Flow* number, where the main regions in it, such as VC, $S33$ and $L33$ structures, were delineated by dimensionless correlations.

From the literature survey, the indistinctness already mentioned can be found regarding the transition from the VC structure to the large cavities structure. An approach of Warmoeskerken and Smith (1985), also assumed by Nienow (1977, 1990), combines cavity structures with empiricism to give the following relationship in dimensionless form. The VC structure is limited by the condition $0 < Fl < Fl_{S33}$.

$$Fl_{S33} = 3.8 \times 10^{-3} (Re^2/Fr)^{0.07} (T/D)^{0.5} \tag{5}$$

where Re denotes Reynolds number, Fr is the Froude number, T is the vessel diameter (m) and D is the impeller diameter (m). The $S33$ structure is limited by the condition $Fl_{S33} < Fl < Fl_{L33}$, where

$$Fl_{L33} = 0.1. \tag{6}$$

Finally, the $L33$ structure is present up to the flooding condition Fl_F given by Nienow et al. (1985)

$$Fl_F = 30 Fr (T/D)^{-3.5}. \tag{7}$$

A criterion of complete dispersion given by Nienow et al. (1977) defines the maximum gas-flow rate at which a given impeller speed will recirculate gas throughout a standard vessel

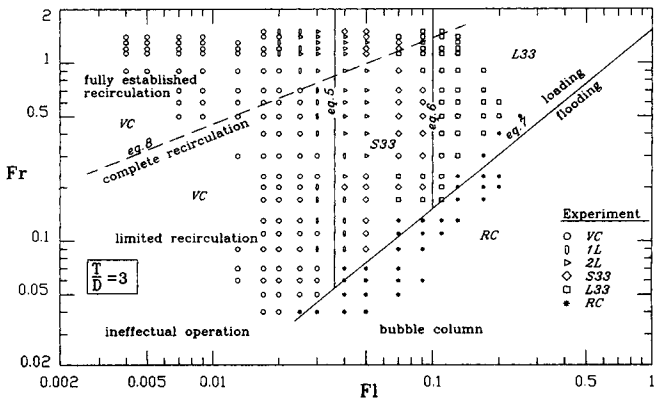

Figure 5. Cavity structures: measured (symbols) vs. predicted by eqs. 5-7: H/T = 1, c/T = 1/3 in D/T = 1.3.

$$Fl_{CD} = 13Fr^2(T/D)^{-5}. \tag{8}$$

The given correlations are plotted in Figure 5 in terms of *Fr-Fl* and under the condition $T/D = 3$. This flow regime map contains structures predicted by Warmoeskerken (1985) marked with lines, a criterion of complete dispersion given by Nienow et al. (1985), and our experimental results of cavity recognition marked with symbols.

The area of *VC* structure corresponds to the given correlations, especially in the area of limited recirculation. In fully established recirculation the $1L$ structure extends into the *VC* structure, as was predicted by Eq. 8. The $2L$ structure appears inside the *S*33 structure in limited circulation. In fully established circulation $2L$ appears even inside the *VC* structure. From the flow map, a flooding transition can be seen for most given *Fr* numbers in the direction of increasing flow rate (at $n = \text{const.}$). Here, hysteresis effects were not studied. Delimitation of the *L*33 and *RC* is in rather close agreement with the criterion of Nienow et al. (1985).

Accordiong to many literature sources, $1L$ and $2L$ structures were detected either in a very narrow range of gas-flow rates (Bruijn et al., 1974; Warmoeskerken and Smith, 1982) or treated as unstable structures (Warmoeskerken and Smith, 1982). Lu and Ju (1989) did show $1L$, $2L$ and '3-3' structures but only at two impeller speeds and with too little data for systematic classification into a flow regime map. Measurements in this work showed that the area of $1L$ and $2L$ structures in the *Fr-Fl* diagram is quite significant, sitting between the *VC* and *S*33 structures. Comparing the predicted structures with our experimental results leads to the conclusion that good agreement is achieved when the impeller operates below complete recirculation; otherwise the situation is a little more complex. In fully established recirculation all measured structures were detected at lower flow numbers than those predicted.

Void fraction distribution

Three basic structures, described in Bombač (1994) were studied in detail:

(a) *L*33 structure at $n = 4.43\ \text{s}^{-1}$ and $q = 1.67 \times 10^{-3}\ \text{m}^3/\text{s}$, using annular (A) or ring (R) sparger.

(b) *S*33 structure at $n = 6.27\ \text{s}^{-1}$ and $q = 1.67 \times 10^{-3}\ \text{m}^3/\text{s}$, using A or R sparger.

(c) *VC* structure at $n = 6.27\ \text{s}^{-1}$ and $q = 5.56 \times 10^{-4}\ \text{m}^3/\text{s}$, using R sparger.

The tabulated α data are available at the authors' address.

The contours of constant void fraction for *L*33 and *S*33 with annular sparger at $c = T/3$ are given in Figures 6a and 6b, respectively. The selected measurement grid allowed us to follow void fraction gradients up to 12% voidage. An annular sparger was chosen to bring the gas directly into the impeller so that the amount of free undispersed gas (region A in Figure 6) between the sparger and the impeller was minimized. Dispersion was carried out first in the *L*33 structure, as shown in Figure 6a, where the liquid discharge flow (as reported by Lu and Ju, 1989) was rather weakened. The reduced liquid pumping capacity of the agitator caused by large cavities resulted in a weak two-phase circulation in the liquid bulk, especially below the impeller (region C), where approximately 30% of liquid bulk remained undispersed. The reason for that can be found in the flow entering the impeller in region A, which comprised a high proportion of air. A weak circulation can be confirmed by contours of discharge flow in region B, which was oriented upward towards the free surface. Above the impeller, the void fraction increased from the vessel wall to the shaft and to the free surface, where it reached maximum value.

By increasing the impeller speed to $n = 6.27\ \text{s}^{-1}$ at $q = 1.67\ 10^{-3}\ \text{m}^3/\text{s}$, a transition from *L*33 to *S*33 occurred (Figure 6b). The recirculation became more intensive; discharge flow in region B tended to expand radially. Upon reaching the vessel wall, the discharge flow split into circulation which

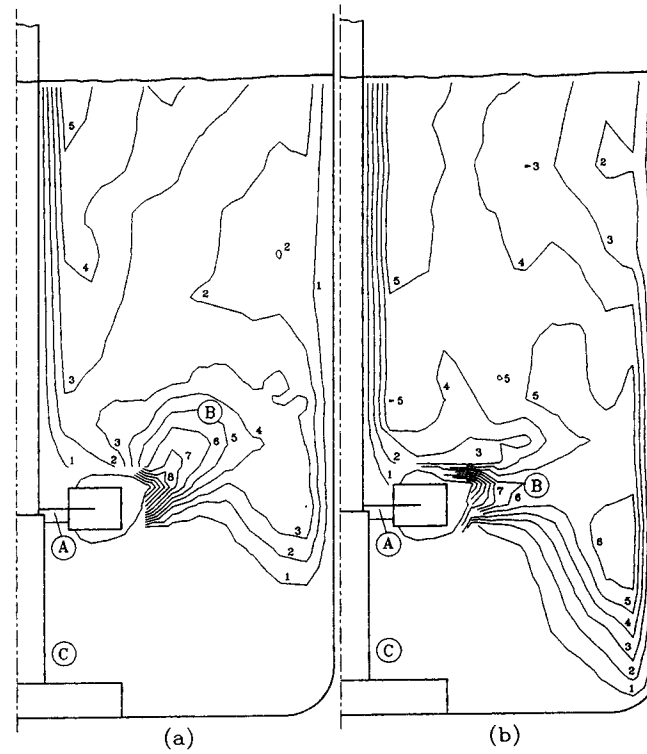

Figure 6. Contours of constant α (%): (a) *L*33; (b) *S*33 by annular sparger with $c/T = 1/3$.

spread below the impeller. This caused considerable increase of dispersed liquid bulk and consequently a significant contribution in the volume integrated value $\langle \alpha \rangle_V$. This circulation was also confirmed by visual observation. Despite more intensive discharge flow compared to $L33$, a large part of the liquid bulk, region C, still remained undispersed. Above the impeller, most of the gas was in both cases concentrated around the shaft. There was a sharper decrease towards the vessel wall compared to $L33$.

To compare the same '3-3' regimes in different conditions, a ring sparger at clearance (m) $c = T/4$ was also analyzed. Contours of $\alpha = \text{const.}$ for different regimes are shown in Figure 7. Using the ratio of one-fourth of the vessel diameter, the undispersed liquid bulk below the impeller was reduced remarkably in all hydrodynamic regimes. The flow entering the impeller from the bottom was single phase with sporadic bubbles only, so that the pumping capacity of the impeller was higher than that with an annular sparger. The result is more intensive gas distribution in the whole liquid bulk. The evolution of discharge flow contours, in region B over *VC*, *S*33 and *L*33 regimes, showed the influence of vertical bubble drift due to buoyancy. In the *VC* regime, contours with sharp (narrow) peaks at the disk level indicated strong two-phase radial flow. Increasing the gas-flow rate in *S*33 increased the discharge flow from the impeller outward. In both *VC* and *S*33 regimes, a discharge flow split into circulation near the vessel wall which spread below the impeller. In *L*33, a skewed profile of discharge flow occurred with a peak at the upper blade edge which generated circulation above the impeller. Single phase with sporadic bubbles only was found in region C in all cases (Figures 7a–7c). Both *L*33 and *S*33 regimes exhibited the majority of the void fraction above the impeller around the shaft (Figures 7b and 7c), whereas in the *VC* regime (Figure 7c) gas was distributed more uniformly.

Reproducibility. The reproducibility was checked under all hydrodynamic conditions occurring in this work: annular and ring sparger by vortex-clinging structure (*VC*), small '3-3' structure (*S*33) and large '3-3' structure (*L*33), in particular (r, z) points. A set of 21 measurements of α was executed with relative reproducibility error smaller than 4%. An example at $r = 94$ mm showed reproducibility for two successive sets of measurements as shown in Figure 8. Error bars are proportionate to the symbol size.

Directional Sensitivity of the R-probe. The directional sensitivity of the R-probe was tested at a chosen location in the (r, z) plane of the *L*33 regime where the motion of bubbles in the upper part of the vessel was very similar to the upward

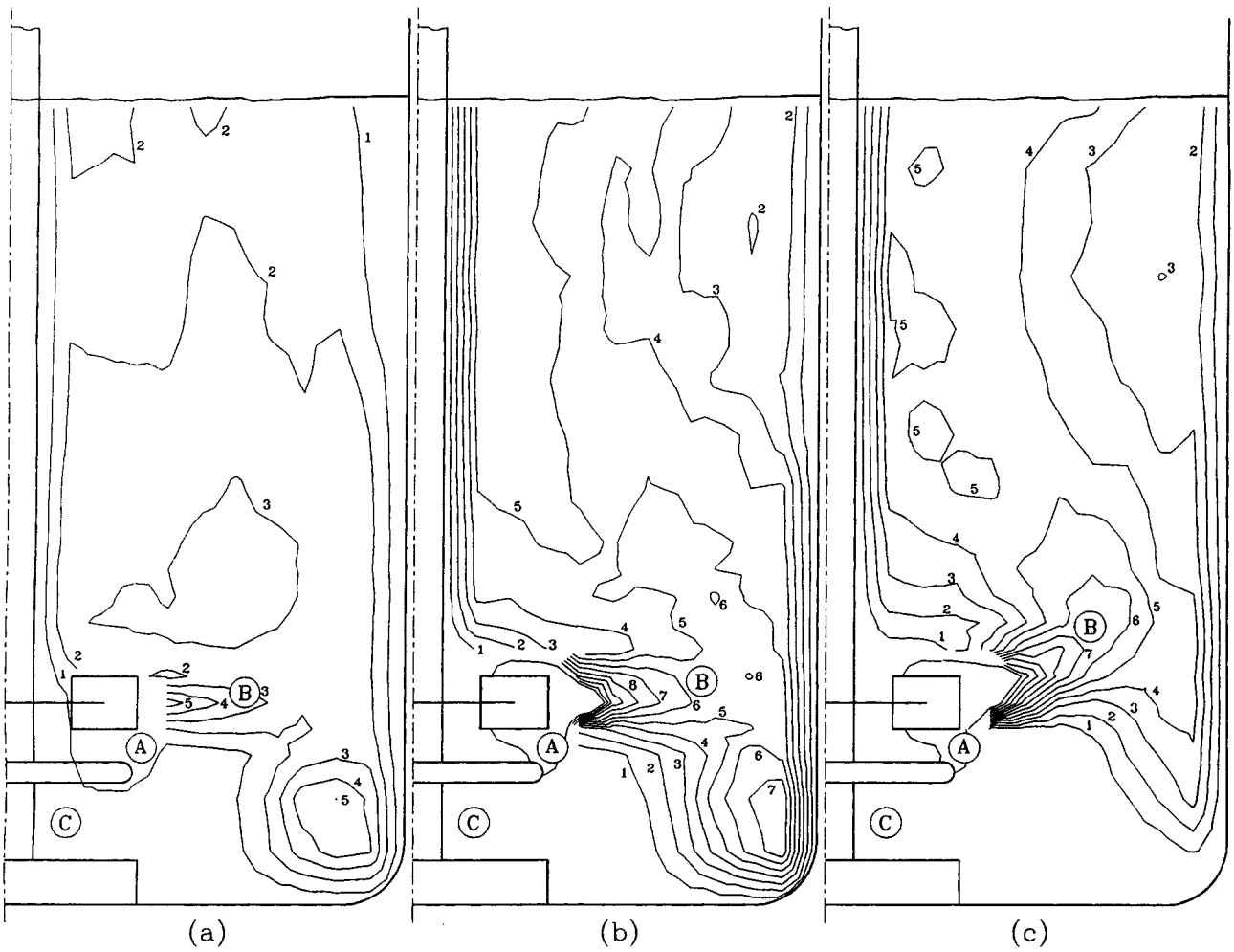

Figure 7. Contours of constant α (%): (a) *VC*; (b) *S*33; (c) *L*33 by ring sparger with $c/T = 1/4$.

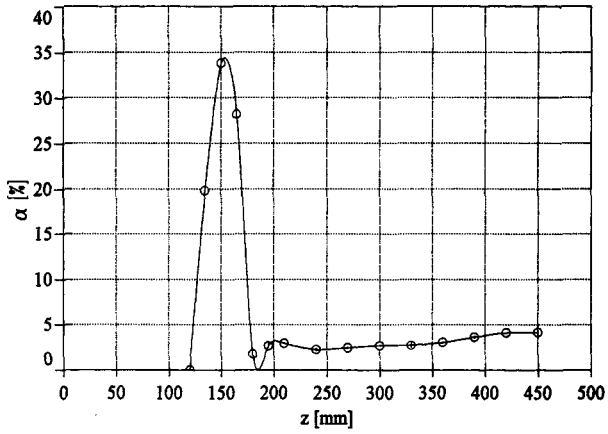

Figure 8. Reproducibility of measurements.

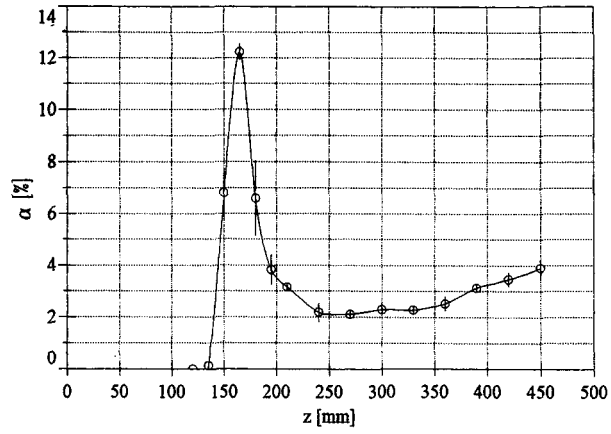

Figure 10. Vertical profiles of α (%) at $\phi = 0°$, 90° and 180°.

bubbly flow in a pipe. α was measured at various impact angles θ, as shown in Figure 9. It was found that the directional sensitivity became significant at impact angles beyond 90°. The relative reproducibility of 20 measured values of α at ϑ smaller than $|90°|$ was found to be within 2.3% and for ϑ between $|90°|$ and $|120°|$ within 10%.

Axial symmetry of α. To check the axial symmetry of the α in the liquid bulk, measurements were conducted at $r = 92$ mm and azimuths $\phi = 0°$, 90°, 180°, under the same hydrodynamic conditions, respectively. Vertical profiles of α in Figure 10 proved that good axis-symmetric two-phase flow was achieved.

Qualitative comparison of α *measured structures with numerical simulations*

In Figure 11a the pattern of measured contours of $\alpha =$ const. is compared to the predicted contours, Figure 11b, as simulated by Bakker and van den Akker (1991). Although the experimental setup scale and cavity regime were equal, the differences in rotational impeller speed n, superficial velocity v_s, sparger clearance c, as well as the shaft bearing in the vessel bottom prevent quantitative comparison of α. There is a basic distinction between the two patterns, however, in the circulation below the impeller close to the vessel wall (Figure 11a), while the same cannot be said for the simulated contours (Figure 11b). The measured values of α, in region C (see Figure 11a), are close to zero. Therefore, it is hard to believe that any gas reaches region C in such high concentration as shown by simulated contours (Figure 11b). The even higher void fraction of the bulk below the impeller than the void fraction of the rest bulk appears to be in contradiction with the results of measured contours (Figure 11a). The same may be concluded when comparing the results of Nienow et al. (1977). Contours of simulated α in the discharge flow from Figure 11b indicate very high void fraction, which we were not able to confirm even at higher impeller speeds. In Figure 11a the distribution of α above the stirrer is rather uniform with a sharp increase at the vessel wall and at the shaft, while from Figure 11b the main part of the void fraction seems to

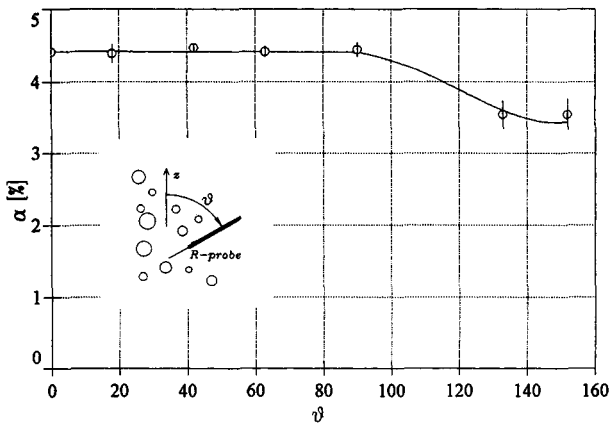

Figure 9. Directional sensitivity of the R-probe.

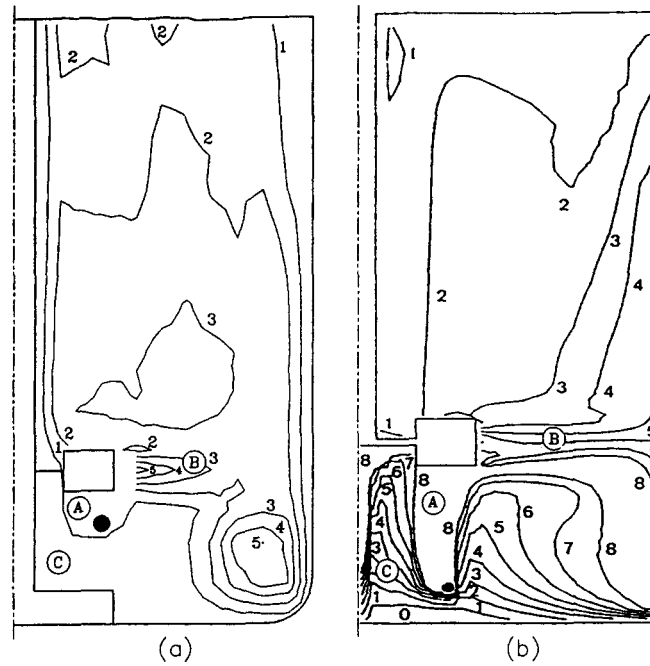

Figure 11. Contours of constant α [%]: (a) based on measurements; (b) predicted by Bakker and van den Akker (1991).

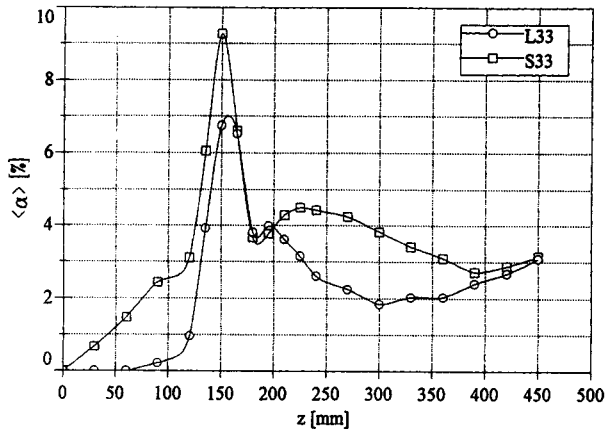

Figure 12. Radially integrated $\langle \alpha \rangle_r$ (%) as a function of height in the case of an annular sparger.

be near the vessel wall. Common to both Figures 11a and 11b is the fact that the void fraction contours imply that the rising gas from the sparger is sucked into the impeller in region A.

Comparison of radially integrated α

Radially integrated values of $\langle \alpha \rangle_r$ are given in Figure 12 for the annular sparger, and in Figure 13 for the ring sparger. Both figures expose characteristic void peaking at impeller location due to discharge flow in all regimes. In the *VC* and *S*33 regimes, where discharge flow is radially oriented, the peak occurs at 150 mm which corresponds to the impeller disk position. In the *L*33 regime where the discharge flow is oriented upward, the peak shifts to the height of the upper blade edge, which can be confirmed by the contours of discharge flow in Figures 6 and 7. A second, less profound peak occurred above the impeller in all cases. This can be explained by recirculation flow produced by the impeller as discussed by Nagase and Yasui (1983). On the other hand, Calderbank (1958) also observed two peaks in the vertical distribution with different gas rates. The *VC* regime in Figure 13 can be taken as an example of void fraction contribution to flow recirculation in $\langle \alpha \rangle_r$. Beside the two already mentioned peaks, another peak occurs below the impeller. This peak clearly indicates recirculation below the impeller (see Figure 6a), which was confirmed by visual observation. In the upper half of the vessel, $\langle \alpha \rangle_r$ decreases with height and reaches a minimum in all regimes (see Figures 12 and 13). These minima are probably due to upward bubble motion. A further increasing of $\langle \alpha \rangle_r$ with the highest value close to the surface layer appears in the *L*33 and *S*33 regimes. This can be explained by hydrodynamic interaction between the rising bubbles and the foaming surface layer.

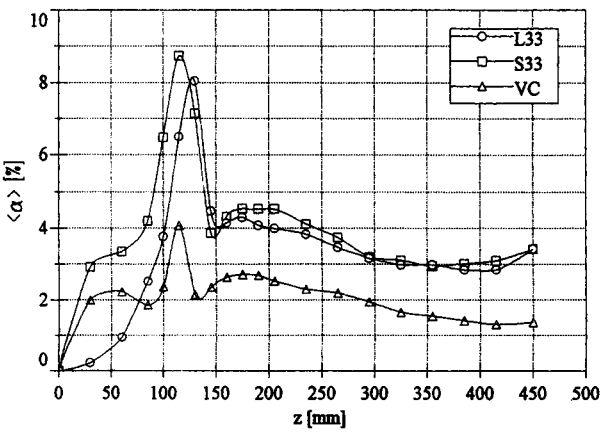

Figure 13. Radially integrated $\langle \alpha \rangle_r$ (%) as a function of height in the case of a ring sparger.

Volume-integrated α vs. global void fraction

The results of volume-integrated values $\langle \alpha \rangle_V$ of α for the discussed regimes are shown in Table 1. Remarkably higher α_G and $\langle \alpha \rangle_V$ were achieved with the ring sparger at $c = T/4$ than with the annular sparger at $c = T/3$. Gas holdup α_G was measured for the given regimes and configurations to be compared with the volume integrated values $\langle \alpha \rangle_V$. Relative small differences in

$$E = \frac{(\alpha_G - \langle \alpha \rangle_V)}{\alpha_G} \tag{9}$$

which were within limits between 4% and 9% confirm the applicability of the entire experimental method (R-probe with phase discrimination method) and the accuracy of α in such nonhomogeneous two-phase systems.

Since the estimated values of gas filled cavities may reach higher values than 12%, which was the upper limit for following the α gradient, the uncertainty estimate was made based on extrapolation of α data close to the impeller. Varying α values between $\alpha_{\text{measured}} \leq \alpha_{\text{est}} \leq 1$ lead to the relative error of the volume integrated (over the entire vessel) values of less than 0.5%.

Comparison of global void fraction

A comparison of global void fraction with the values available in the literature is difficult due to different setup scales, geometry and measurement techniques (Table 2). No general correlation of global void fraction is available which would predict α_G with sufficiently high accuracy. A number of equations have been proposed for α_G, such as by Hassan and Robinson, Yung et al., after Mann (1983) and Greaves and Barigou (1987) and Smith (1991), which are shown in Table 3.

Table 1. Comparison of Volume-Integrated $\langle \alpha \rangle_V$ and Global α_G

Regime	*L*33	*S*33	*VC*
(n, q) [min^{-1}, 1/h]	266, 6000	376, 6000	376, 2000
Annular Sparger			
$\langle \alpha \rangle_V$	2.2%	3.4%	—
α_G	2.4%	3.6%	—
E	0.07	0.04	—
Ring Sparger			
$\langle \alpha \rangle_V$	3.2%	3.8%	2.0%
α_G	3.3%	4.2%	2.2%
E	0.04	0.08	0.09

$E = (\alpha_G - \langle \alpha \rangle_V)/\alpha_G$.

Table 2. Experimental Conditions for Global or Local Void Fraction Measurements

Author/Geom. Par.	T (m)	D/T	c/T	n (rpm)	v_s (mm/s)	P/V (kW/m^3)	ST	MM
Hassan and Robinson*	0.15–0.29	—	—	—	—	0.3–1.62	—	ll
Nienow et al. (1977)	0.29	1/3	1/4	228–474	1–12	—	pipe	sm
Yung et al.*	0.40	—	—	—	—	0.8–5.0	—	im
Nagase and Yasui (1983)	0.25	1/2	1/3	287	—	—	ring	sm
Greaves and Barigou (1987)	1.0	1/4–1/2	1/4	40–500	—	—	pipe	sc
Bakker and van den Akker (1991)	0.44	1/4	1/3	333	3.6	1.52	ring	op
Smith (1991)	0.44–4.2	1/4–1/2	1/4–1/3	—	—	—	—	mc
This work	0.45	1/3	1/4, 1/3	267, 376	3.6, 10	0.48, 1.39	ring	rp

*Cited by Mann (1983).
Legend: ST—sparger type; MM—measuring method; mc—measuring cylinder; sc—set of conductivity probes; op—optical probe; sm—suction method; rp—resistivity probe; ll—liquid level; im—inclined manometer.

Table 3. Comparison of Measured Gas Holdups with Correlated Values for Given Regimes

Researchers	Equation	$L33$	$S33$	VC
Hassan and Robinson*	$\alpha_G = 0.113 n^{1.14} q^{0.57} \sigma^{-0.57}$	7.2	10.7	5.7
Yung et al. (1979)	$\alpha_G = 0.52 Fl^{1.14} \mathrm{We}^{0.65} (D/T)^{1.4}$	3.14	4.16	2.4
Greaves and Barigou (1987)				
VC regime	$\alpha_G = 3.85 n^{0.73} q^{0.62} (D/T)^{1.64}$	—	—	2.3
Large cavity regime	$\alpha_G = 1.33 n^{0.60} q^{0.44} (D/T)^{1.33}$	4.6	4.7	—
Smith (1991)	$\alpha_G = 0.85 (Re \cdot Fr \cdot Fl)^{0.35\ 1.25}$	3.7	4.7	3.2
Our measurements		3.3	4.2	2.2

*Cited by Mann (1983).

Hassan and Robinson and Yung et al. proved that the surface tension is of great importance; Greaves and Barigou (1987) introduced separate criteria to calculate α_G according to the appearance of gas-filled cavity types and reduced the uncertainty band considerably. Smith's correlation of global gas retention in an aerated tank is based on measurements on different scales of reactors such as $0.44 \leq T \leq 4.2$ [m]. Introducing the product of the dimensionless numbers $Fr \cdot Fl \cdot Re$, the prediction becomes independent of scale, and accurate at holdups lower than 10%.

In this work the holdup α_G was measured using the ring sparger, and was found to be within the limits of the values of the above mentioned criteria.

Conclusions

The gas-filled cavities present at the Rushton disk impeller were detected using a microresistivity probe. The experimental method based on a time-domain structural function and on its frequency transformation enables cavity structure recognition, such as the vortex-clinging structure, the appearance of the first large cavity, two large cavities, small '3-3' structure, large '3-3' structure and ragged cavities RC. The method proved to be simple and effective. Recognized structures, classified into a flow regime map, indicate good agreement with those predicted from literature, especially in limited recirculation. In fully established recirculation, measured structures were detected at lower flow numbers than those predicted. It was found that the transition area between the VC and $S33$ structures may be larger than was evident from the literature. This was explained with structures $1L$ and $2L$.

Local void fraction was measured at 190 nodes in the vertical half-section plane of the vessel. The data matrix can be used as input parameters for (or verification of) CFD predictions. From the contours of α, an influence of bubble buoyancy on the two-phase flow direction can be seen in all regimes, as well as a tendency of bubbles to concentrate around the shaft above the impeller. This is the first time that α were measured and compared with gas holdups in a pilot-size aerated stirred vessel.

Relatively small differences between integrated values of α and measured gas holdups confirm the applicability of the entire experimental method (R-probe with phase discrimination), and the reliability of α in such nonhomogeneous two-phase systems. The insensitivity of the R-probe to two-phase flow direction over a wide impact angle enables reasonable accuracy of measured α in an aerated stirred tank under hydrodynamic regimes, that is, vortex-clinging, small '3-3', and large '3-3' structure.

From the radially integrated values of α in the r-z plane, characteristic void peaking at different heights can be seen. The maximum is achieved at the level of the impeller due to discharge flow. Other, less profound peaks occurred above and below the impeller and can be explained by recirculation flow.

Notation

b = blade length, m
d = disk diameter, m
f = baffle width, m or blade frequency, s^{-1}
g = gap between the vessel wall and the baffle, m or gravity, m/s^2
H = liquid height, m
P = ungassed power, W
q = volumetric gas flow rate, m^3/s
r, z = coordinates, m
R = radius of the bottom edges, m
s = sparger clearance above the base, m
t = total time, s
Δt_{Li} = liquid-phase residence time, s
v_s = superficial velocity, $4q/\pi T^2$, m/s

V = tank liquid volume, m^3
w = blade width, m
Fl = Flow no., q/nD^3
Fr = Froude no., Dn^2/g
Re = Reynolds no., $dD^2\rho/\mu$
We = Weber no., $\rho n^2 D^3/\sigma$
$\langle \alpha \rangle_r$ = radially integrated void fraction
ρ = density, kg/m^3
σ = surface tension, N/m
μ = viscosity, Pa·s

Acknowledgments

This work was financially supported by the Slovenian Ministry of Science and Technology under contract No. P2-5095-0782. The assistance of M. Livk who implemented a computer program for drawing contours is gratefully acknowledged.

Literature Cited

Bakker, A., and H. E. van den Akker, "A Computational Study on Dispersing Gas in a Stirred Reactor," *Fluid Mechanics of Mixing*, R. King, ed., Kluwer Academic Publisher, p. 37 (1991).

Barigou, M., and M. Greaves, "Bubble Size in the Impeller Region of a Rushton Turbine," *Trans. I Chem. E.*, **70**, Part A, 153 (Mar. 1992).

Bombač, A., "Interfacial Structure Characteristics in an Aerated Stirred Vessel," PhD Thesis, Faculty of Mechanical Engineering, Univ. of Ljubljana (1994).

Bombač, and I. Žun, "Detection of Loading-Flooding Transition in an Aerated Stirred Vessel," *Proc. Kuhljevi dnevi*, (in Slovene), Portorož, Slovene Soc. of Mechanics, p. 123 (1992).

Bruijn, W., K. van't Riet, and J. M. Smith, "Power Consumption with Aerated Rushton Turbines," *Trans. Instn. Chem. Engrs.*, **52**, 88 (1974).

Calderbank, P. H., "Physical Rate Processes in Industrial Fermentation," *Trans. Instn. Chem. Engrs.*, **36**, 443 (1958).

Cartellier, A., and J. L. Achard, "Local Phase Detection in Fluid/Fluid Two-Phase Flows," *Rev. Sci. Instrum.*, **62**(2), 279 (1991).

de Figueiredo, M. M. L., and P. H. Calderbank, "The Scale-up of Aerated Mixing Vessels for Specified Oxygen Dissolution Rates," *Chem. Eng. Sci.*, **34**, 1333 (1979).

de More, L. S., W. F. Pafford, and G. B. Tatterson, "Cavity Sound Resonance and Mass Transfer in Aerated Agitated Tanks," *AIChE J.*, **34**, 1922 (1988).

Frijilink, J. J., "Physical Aspects of Gassed Suspension Reactors," Doctoral Thesis, TU Delft, The Netherlands (1987).

Gosmann, A. D., C. Lekakou, S. Polis, R. I. Issa, and M. K. Looney, "Multidimensional Modeling of Turbulent Two-Phase Flows in Stirred Tanks," *AIChE J.*, **38** (12), 1946 (1992).

Greaves, M., and M. Barigou, "Estimation of Gas hold-up and Impeller Power in a Stirred Vessel Reactor," *I. Chem. E. Symp. Ser.*, No. 108, p. 235 (1987).

Ishii, M., *Thermo-Fluid Dynamic Theory of Two-Phase Flow*, Eyrolles, Paris (1975).

Ismail, A. F., Y. Nagase, and J. Imon, "Power Characteristics and Cavity Formation in Aerated Agitations," *AIChE J.*, **30** (3), 487 (1984).

Lu, W. M., and S. J. Ju, "Cavity Configuration, Flooding and Pumping Capacity of Disk-type Turbines in Aerated Stirred Tanks," *Chem. Eng. Sci.*, **44**(2), 333 (1989).

Mann, R., "Gas-Liquid Contacting in Mixing Vessels," *IChemE*, Rugby, England (1983).

Morud, K. E., and B. H. Hjertager, "LDA Measurements and CFD Modelling of Gas-Liquid Flow in a Stirred Tank," *Chem. Eng. Sci.*, **51**(2), 233 (1996).

Nagase, Y., and H. Yasui, "Fluid Motion and Mixing in a Gas-Liquid Contactor with Turbine Agitators," *Chem. Eng. J.*, **27**, 37 (1983).

Nienow, A. W., "Gas Dispersion Performance in Fermentor Operation," *Chem. Eng. Prog.*, 61 (Feb. 1990).

Nienow, A. W., D. J. Wisdom, and J. C. Middleton, "The Effect of Scale and Geometry on Flooding, Recirculation, and Power in Gassed Stirred Vessels," *Proc. Eur. Conf. on Mixing*, Paper F1, Cambridge (1977).

Nienow, A. W., M. M. C. G. Warmoeskerken, J. M. Smith, and M. Konno, "On the Flooding/Loading Transition and the Complete Dispersal Condition in Aerated Vessels Agitated by a Rushton-Turbine," *Proc. Eur. Conf. on Mixing*, Wurzburg, Paper 15 (1985).

Ranade, V. V., and H. E. A. van den Akker, "A Computational Snapshot of Gas-Liquid Flow in Baffled Stirred Reactor," *Chem. Eng. Sci.*, **49** (24B), 5175 (1994).

Rushton, J. H., and J. J. Bimbinet, "Holdup and Flooding in Air Liquid Mixing," *Can. J. Chem. Eng.*, **46**, 16 (1968).

Smith, J. M., "Simple Performance Correlations for Agitated Vessels," *Fluid Mechanics of Mixing*, R. King, ed., Kluwer Academic Publisher, p. 55 (1991).

Smith, J. M., M. M. C. G. Warmoeskerken, and E. Zeef, "Flow Conditions in Vessel Dispersing Gases in Liquids with Multiple Impellers" *Biotechnology Processes*, C. S. Ho and J. Y. Oldshue, eds., AIChE, p. 107 (1987).

Takahashi, K., and A. W. Nienow, "Vortex Cavity Shape and the Associated Path-Line of Discharged Bubbles in an Aerated Vessel Agitated by a Rushton Turbine," *J. Chem. Eng. Jpn.*, **25** (5), 539 (1992).

van't Riet, K., and J. M. Smith, "The Behavior of Gas-Liquid Mixtures Near Rushton Turbine Blades," *Chem. Eng. Sci.*, **28**, 1031 (1973).

Warmoeskerken, M. M. C. G., and J. M. Smith, "Description of the Power Curves of Turbine Stirred Gas-Liquid Dispersions," *Proc. Eur. Conf. on Mixing*, Paper G1, Noordwijkerhout, The Netherlands (1982).

Warmoeskerken, M. M. C. G., and J. M. Smith, "Flooding of Disk Turbines in Gas-Liquid Dispersions: A New Description of the Phenomenon," *Chem. Eng. Sci.*, **40** (11), 2063 (1985).

Žun I., I. Kljenak, and S. Može, "Space-Time Evolution of the Nonhomogeneous Bubble Distribution in Upward Flow," *Int. J. Multiphase Flow*, **19**, 151 (1993).

Žun, I., B. Filipič, M. Perpar, and A. Bombač, "Phase Discrimination in Void Fraction Measurements Via Genetic Algorithms," *Rev. Sci. Instrum.*, **66**(10), 5055 (1995).

Manuscript received July 29, 1996, and revision received April 14, 1997.